Progress In Electromagnetics Research C, Vol. 172, 275–285, 2026

PIER C

(Received 26 June 2026, Accepted 20 July 2026, Scheduled 11 August 2026)

Accounting for a Single Reflected Path in Antenna Array Field Focusing

Denis Iuzvik* and Maksim Stepanov

Novosibirsk State Technical University, 630073, Russian Federation

ABSTRACT: A low-complexity first-order model was developed and verified to account for a single reflected propagation path in the complex transmission-coefficient matrix used for electromagnetic-field focusing by an antenna array. Electrodynamic and mathematical modeling was performed for a system comprising a transmitter, a receiving point, and an ideal specular reflector represented as a scattering point. The reflected-path contribution was incorporated directly into the transmission coefficients used to calculate the complex excitations of antenna-array radiators. The approach was evaluated using a three-element antenna array by comparing field focusing without a reflector, with an uncompensated reflector, and with reflector-aware excitation parameters. Changes in reflector position altered phase difference between direct and reflected waves, resulting in constructive or destructive interference at the receiving point. Taking the reflected path into account modified the calculated amplitudes and initial phases of the array excitations and partially compensated for reflector-induced field distortion. In the considered case, the normalized field amplitude after compensation differed by approximately 3% from the no-reflector case and increased by about 49% relative to the uncompensated case. The mathematical and electrodynamic results were in qualitative agreement. These findings demonstrate that including a reflected path in a transmission-coefficient matrix can improve near-field focusing accuracy in the presence of a reflector.

1. INTRODUCTION

Control of the spatial distribution of an electromagnetic field is an important problem in microwave engineering and wireless communications. In confined environments, the ability to create a localized field maximum at a prescribed point can improve the signal-to-noise ratio and support more efficient spatial reuse of the radio channel. This is particularly relevant to dense wireless networks, where devices operating in the same frequency band may interfere with one another and reduce the achievable data transmission rate [1, 2].

When the target point is located in the radiating near field of an antenna array, conventional far-field beam steering is insufficient. In the far field, the wavefront can usually be approximated as planar, and beam control is performed mainly in the angular domain. In the near field, however, the spherical nature of the wavefront and distance-dependent phase must be taken into account. Consequently, the complex excitations of the array elements must be selected to provide focusing not only in angle but also in range [3, 4].

In real indoor and confined environments, electromagnetic-wave propagation is affected by walls, furniture, equipment, and other reflecting objects. The field at the receiving point is therefore formed by the superposition of the direct wave and reflected, diffracted, or scattered components. Depending on their relative phases, these components may enhance the desired field maximum or reduce it through destructive interference. Ray-tracing methods are widely used to describe such propagation scenarios because they can account for direct paths, specular reflections, diffraction, scattering, and propagation losses [5]. However, ray tracing is generally used as a forward propagation tool: the transmitter parameters are specified, and the resulting channel or field distribution is calculated.

The present study addresses a related but different problem. The reflected path is included directly in the mathematical procedure used to calculate the complex excitations of the antenna-array radiators. Thus, the objective is not only to determine how a reflector changes the field after the array excitations have been specified, but also to determine amplitudes and initial phases that compensate for this influence. Ray tracing may be used to estimate the geometrical and electromagnetic parameters of the reflected paths, whereas the proposed approach uses these parameters within an inverse field-synthesis procedure. Therefore, the proposed model is complementary to ray-tracing techniques rather than a replacement for them.

Electromagnetic time reversal and phase conjugation are also related to the problem of field focusing in multipath environments. In time-reversal systems, the channel impulse response is usually measured or estimated, after which a time-reversed or phase-conjugated signal is transmitted. As a result, multipath components contribute to spatiotemporal energy focusing at the original source or target location [6, 7]. The approach considered in the present study does not involve temporal reversal or retransmission of a measured channel response. Instead, a monochromatic deterministic model is used, in which direct and selected reflected paths are represented explicitly by their propagation lengths, attenuation factors, and complex coefficients. The required radiator excitations are then obtained by solving a system of linear equations.

* Corresponding author: (zetanicestar@gmail.com).

TABLE 1. Comparison of electromagnetic-field focusing and multipath-control approaches.

Method	Reflection modeling	Role in excitation optimization	Multiple targets	Computational cost	Model complexity
Free-space transmission-coefficient method [9, 10]	Reflections are not explicitly included	Complex radiator excitations are calculated using direct-path coefficients	Supported in the general multiport formulation	Low	Low
Ray tracing [5]	Explicit geometrical modeling of reflections, diffraction, and scattering	Primarily forward channel or field calculation; an additional optimization procedure is required	Supported	High for detailed environments	High
Time reversal [6, 7]	Multipath is included implicitly through the measured or estimated channel response	Excitations are obtained by time reversal or phase conjugation	Possible, but requires multi-target channel processing	Moderate to high	Moderate to high
Reconfigurable intelligent surfaces [8]	Reflections are actively controlled by reconfigurable intelligent surface (RIS) elements	Joint optimization of the transmitter and/or reflecting surface is generally required	Supported in advanced formulations	High	High
Proposed method	One reflected path is explicitly included in each effective transmission coefficient	Radiator amplitudes and initial phases are recalculated using the effective coefficient matrix	One target in the present study; extension is possible	Low to moderate	Low

A distinction should also be made between the proposed method and reconfigurable intelligent surfaces. An RIS is designed to modify the radio channel by controlling reflection phase and, in some implementations, the reflection amplitude of its individual elements [8]. In the present study, the reflecting object is passive and time-invariant. Its electromagnetic properties are not controlled or optimized. Compensation is achieved exclusively by changing the complex excitations of the antenna-array radiators, while the reflector is treated as a fixed part of the propagation environment.

The main differences between the considered approaches are summarized in Table 1. The comparison shows that the proposed method is not intended to replace full-wave propagation modeling, time reversal, or RIS-based channel control. Its purpose is to provide a low-complexity algebraic extension of the transmission-coefficient method for calculating antenna-array excitations in the presence of a known reflected path.

As shown in Table 1, the novelty of the proposed method is not the general modeling of multipath propagation. Its contribution is the direct incorporation of a selected reflected path into the same complex transmission-coefficient matrix that is used for antenna-excitation synthesis. This preserves the algebraic structure of the original multiport method and avoids the need for channel sounding, controllable reflecting elements, or repeated full-wave optimization.

The research gap addressed in this study is therefore the absence of a transparent first-order analytical model that incorporates a reflected propagation path directly into the complex transmission-coefficient matrix used for antenna-array excitation synthesis. Existing free-space focusing models do not explicitly include the influence of reflecting objects in the excitation calculation, while conventional ray-tracing methods primarily characterize the propagation channel. Time-reversal techniques and RIS-based systems solve related problems but rely on different physical principles and control variables.

Accordingly, the objective of this study is to develop and verify a mathematical model including one specularly reflected propagation path in the matrix of complex transmission coefficients during electromagnetic-field focusing at a prescribed point. The study's scientific contribution consists of three main elements. First, an analytical expression is formulated for the contribution of a reflected path to the effective transmission coefficient between an antenna-array radiator and the receiving point. Second, the resulting effective coefficient matrix is incorporated into the linear procedure used to calculate the amplitudes and initial phases of the radiator signals. Third, electrodynamic and mathematical modeling are used to demonstrate the influence of the reflected path and to verify the possibility of partial compensation for resulting field distortion.

The study intentionally considers the basic case of a single ideal specular reflector represented as a scattering point. This simplified formulation makes it possible to isolate the phase and amplitude mechanisms associated with the reflected path and to verify the proposed matrix representation. The model is intended as a first-order step toward more general formulations that include several reflectors, multiple reflections, complex material-dependent reflection coefficients, diffuse scattering, and field synthesis within a prescribed spatial region rather than at a single point.

2. ELECTRODYNAMIC MODELING OF A SCATTERING POINT

To understand the influence of a reflecting object on the electric-field distribution in space, we begin by considering the simplest case: one transmitting antenna, one scattering point,

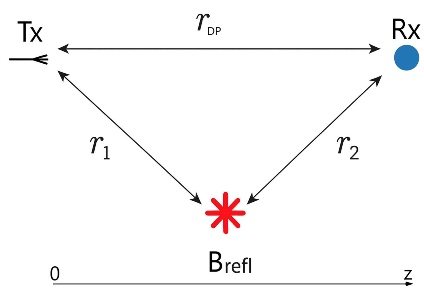

FIGURE 1. Illustration of a system containing a scattering point.

and one receiving point. The operating frequency is 2.5 GHz. A graphical representation of this example is presented in Figure 1.

The example shown in Figure 1 illustrates that there are two propagation paths from the transmitting antenna (Tx) to the receiving point (Rx): the first path is the direct path r_{DP}, and the second path is the propagation path through the scattering point B_{refl}, consisting of path r_1 from the transmitting antenna to the scattering point and path r_2 from the scattering point to the receiving point.

For electrodynamic modeling, let us consider three cases:

1. Electrodynamic modeling of the dependence of the electric-field strength amplitude on a single antenna. The antenna coordinates were $(x = 0; y = 0)$. This case is referred to as the case without a scattering point.
2. Introduction of a scattering point into a system consisting of a single antenna. The coordinates of the scattering point are $(x = 250; y = -125)$, which, given the path difference in the waves, should provide a phase difference at the receiving point Rx $(x = 500; y = 0)$ $\Delta\phi = 180°$.
3. Introduction of a scattering point into a system consisting of a single antenna. The coordinates of the scattering point are $(x = 250; y = -185)$, which, given the path difference in the waves, should provide a phase difference at the receiving point Rx $(x = 500; y = 0)$ $\Delta\phi = 360°$.

Thus, we expect to obtain the following: for case 1, a reference value of the electric-field strength amplitude as a function of distance without the influence of scattering points; for case 2, destructive interference at the point with coordinates $(x = 500; y = 0)$; and for case 3, constructive interference at the point $(x = 500; y = 0)$.

For electrodynamic modeling, a model of the antenna and reflecting object was built with Dassault Systèmes SIMULIA CST Studio Suite 2025. A perfect electric conductor (PEC) was used as the reflecting object. The standard Time Domain Solver based on the finite integration technique was used. This solver was selected because it provides a full-wave transient solution and allows the electromagnetic-field response to be evaluated at the operating frequency from a single time-domain calculation. The background material of the computational domain was vacuum. Open boundary conditions with additional space, Open (add space), were assigned to all six sides of the computational domain to approximate radiation into unbounded free space. The size of the additional free-space region was determined automatically by Computer Simulation Technology (CST) using standard open-boundary settings. The reflecting object was modeled as a perfect electric conductor. The transmitting antenna was excited using a standard waveguide port located at the antenna feed cross-section. Only the fundamental propagating mode of the port was considered. The port mode and its field distribution were calculated automatically by the CST port-mode solver. The standard CST port-amplitude normalization was retained. The computational domain was discretized using the automatically generated hexahedral mesh of the Time Domain Solver. Perfect Boundary Approximation was used to represent the interfaces and curved geometrical features. The global mesh parameters were left at their standard CST values, and the mesh was generated automatically according to the model's dimensions and the shortest wavelength in the specified frequency range. No manual local mesh refinement or additional adaptive mesh passes were applied. The electric-field distribution was evaluated using an electric-field monitor at the operating frequency of 2.5 GHz. The simulations were performed on a workstation equipped with an Intel Core i7 processor and 32 GB of RAM. The typical wall-clock simulation time for one configuration was approximately 40 minutes. The model is illustrated in Figure 2.

Figure 3 shows the dependence of the electric-field strength amplitude without considering the scattering point.

Figure 4 shows the dependence of the electric-field strength amplitude when a scattering point is added to the system, with a phase difference of $\Delta\phi = 180°$.

Figure 5 shows the dependence of the electric-field strength amplitude when a scattering point is added to the system, with a phase difference of $\Delta\phi = 360°$.

Table 2 summarizes values of the electric-field strength amplitude at points corresponding to the receiving point Rx $(x = 500; y = 0)$ and the farther point $(x = 600; y = 0)$.

TABLE 2. Electric field strength amplitudes.

Reflection condition	$\lvert E\rvert$ at $x = 0.5$ m, V/m	$\lvert E\rvert$ at $x = 0.6$ m, V/m
No reflector	27.76	21.19
$\Delta\phi = 180$	16.54	18.56
$\Delta\phi = 360$	38.1	28.65

Analyzing the results of the electrodynamic modeling shown in Figures 3, 4, and 5, as well as the data from Table 2, it becomes clear that the reflecting object, depending on its location, makes it possible to provide a phase difference at the receiving point based on the resulting phase shift caused by the path difference.

3. MATHEMATICAL MODEL

Let us briefly recall the method for forming a single antinode of the electromagnetic field, which follows from [9, 10]. Figure 6 shows a system consisting of several antennas and one receiving point.

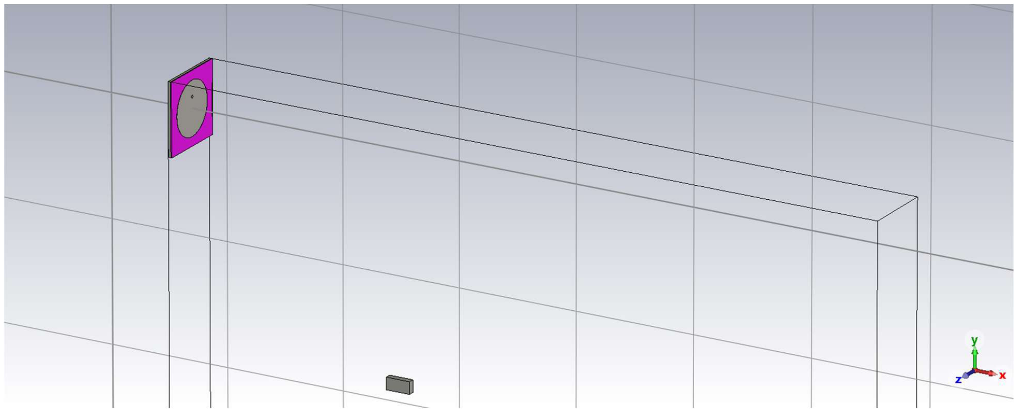

FIGURE 2. Model in Dassault Systèmes SIMULIA CST Studio Suite 2025.

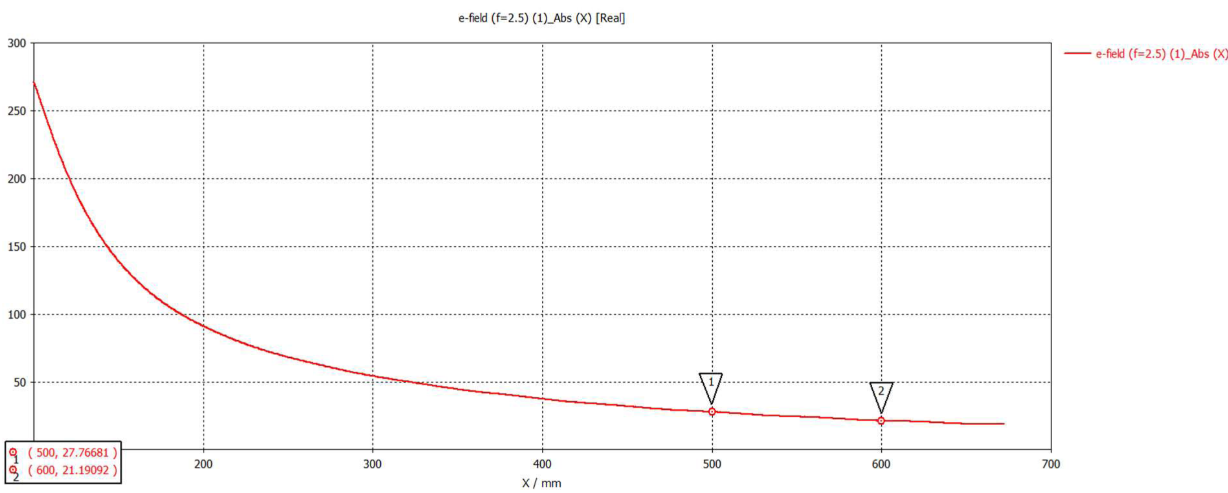

FIGURE 3. Dependence of the electric-field strength amplitude without a scattering point.

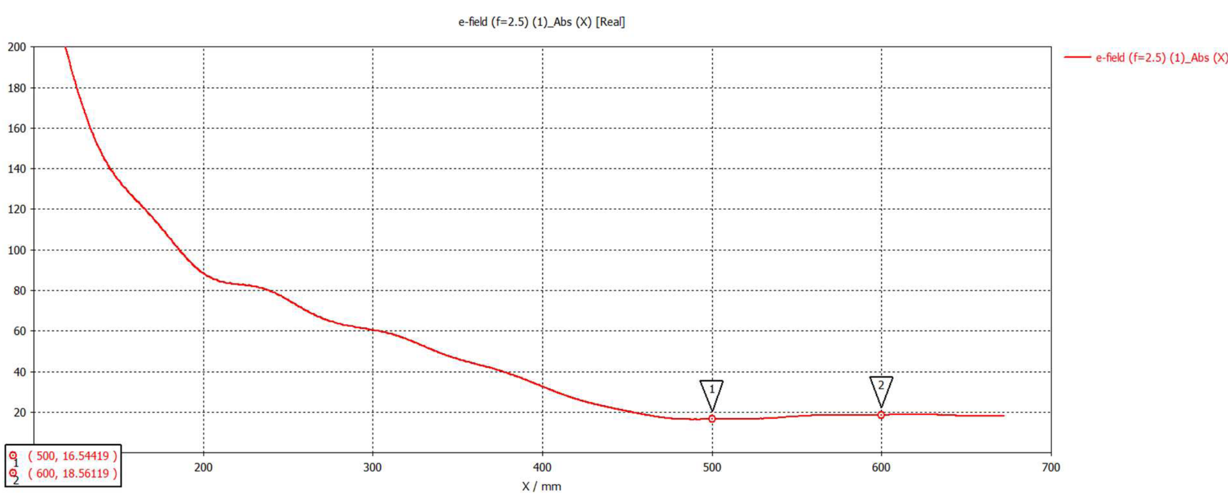

FIGURE 4. Dependence of the electric-field strength amplitude with a scattering point taken into account, $\Delta\phi = 180^{\circ}$.

Let us recall the notation for the complex amplitudes of the transmitted signals from [9]:

$$a_n = |a_n| \cdot e^{j\phi_i}, \tag{1}$$

where $|a_n|$ is the amplitude of the signal emitted from the i-th point; ϕ_i is the initial phase of the signal emitted from the n-th point; and j is the imaginary unit.

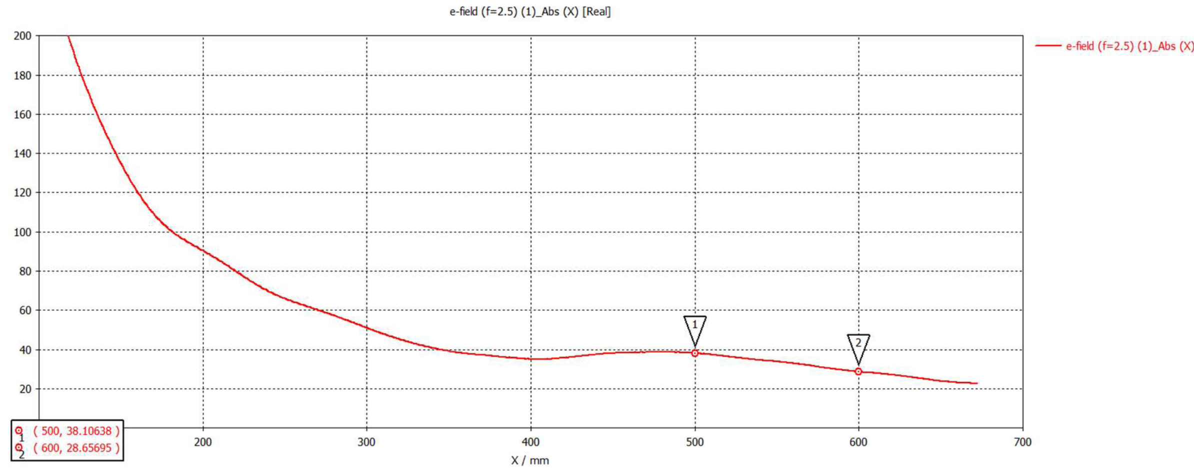

FIGURE 5. Dependence of the electric-field strength amplitude with a scattering point taken into account, $\Delta\phi = 360$.

Complex amplitude at receiving points:

$$b_m = |b_m| \cdot e^{j \cdot \psi_m}, \tag{2}$$

where $|b_m|$ is the signal amplitude at the m-th point, and ψ_m is the signal phase at the m-th point.

The set of complex amplitudes of the signals at radiation points forms a column vector of emitted signals $[A]$, and the set of complex amplitudes of the signals at reception points forms a column vector of received signals $[B]$.

For the system shown in Figure 6 [9], the number of inputs to the multiport network is $N + M$, where N is the number of emitting antennas, and M is the number of receiving points. Obviously, inputs 1 through N correspond to the emitting antennas, and inputs $N + 1$ through $N + M$ correspond to the receiving points.

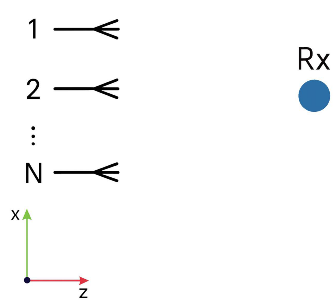

FIGURE 6. System consisting of transmitting antennas and a receiving point.

Therefore, by specifying a column vector of the output signals of the multiport $[Y]$, it is possible to define a column vector of the input signals $[X]$. They are connected by a matrix of direct transmission coefficients $[S_{RT}]$:

$$[Y] = [S_{RT}] \cdot [X], \tag{3}$$

In free space, transmission coefficients are determined by the following expression [9]:

$$s_{i,k} = F_{i,k} \cdot F_{k,i} \cdot r_{i,k}^{-q} \cdot \exp(-j \cdot \beta \cdot r_{i,k}), \tag{4}$$

where $r_{i,k}$ is the distance from the point corresponding to the i-th input of the multiport network to the point corresponding to the k-th input of the multiport network; $\beta = \frac{2 \cdot \pi}{\lambda}$ is the phase coefficient; $F_{i,k}$ are elements of the matrix containing the antenna's field gain coefficients installed at the point corresponding to input k in the direction of the point corresponding to input i; and factor $r_{i,k}^{-q}$ determines the decrease in the amplitude of the electromagnetic wave strength during propagation from the point corresponding to the input of the multiport i to the point corresponding to the input of the multiport k. For the electromagnetic field in the near zone, $q = 2$, and for the electromagnetic field in the far zone, $q = 1$.

The amplitude of the electric-field strength formed by propagation along the direct path (DP) to the k-th point is determined by the following expression [10]:

$$E_k^{(\mathrm{DP})} = \sum_{i=1}^{N} \left[A_i \cdot F_{i,k} \cdot r_{i,k}^{-q} \cdot \exp\left(j \cdot [\beta \cdot r_{i,k} + \phi_i]\right) \right], \tag{5}$$

where A_i is the amplitude of the radiated signal of the i-th antenna; $r_{i,k} = \sqrt{(x_i - x_k)^2 + (y_i - y_k)^2 + (z_i - z_k)^2}$; and ϕ_i is the initial phase of the signal of the i-th antenna.

In Expression (5), the factor $r_{i,k}$ contains the shortest distance between the i-th antenna and the k-th point. It is not difficult to guess that the propagation path from the transmitting antenna to the receiving point through the scattering point will include distances r_1 and r_2. We can write an expression for determining the amplitude of the electric-field strength at the reception point, which is formed by propagation only through the scattering point (Bright Path):

$$\begin{aligned} E_k^{(BP)} \; = \; & \sum_{i=1}^{N} \left[A_i \cdot F_{i,b} \cdot \Gamma_{b,k} \cdot (r_{i,b} + r_{b,k})^{-q} \right. \\ & \left. \cdot \exp\left(j \cdot [\beta \cdot (r_{i,b} + r_{b,k}) + \phi_i]\right) \right], \end{aligned} \tag{6}$$

where $F_{i,b}$ is the field gain of the i-th antenna towards the b-th scattering point; $\Gamma_{b,k}$ is the complex reflectivity between the b-th scattering point and the k-th point; $r_{i,b}$ is the distance between the i-th antenna and the b-th scattering point; and $r_{b,k}$ is the distance between the b-th scattering point and the k-th point.

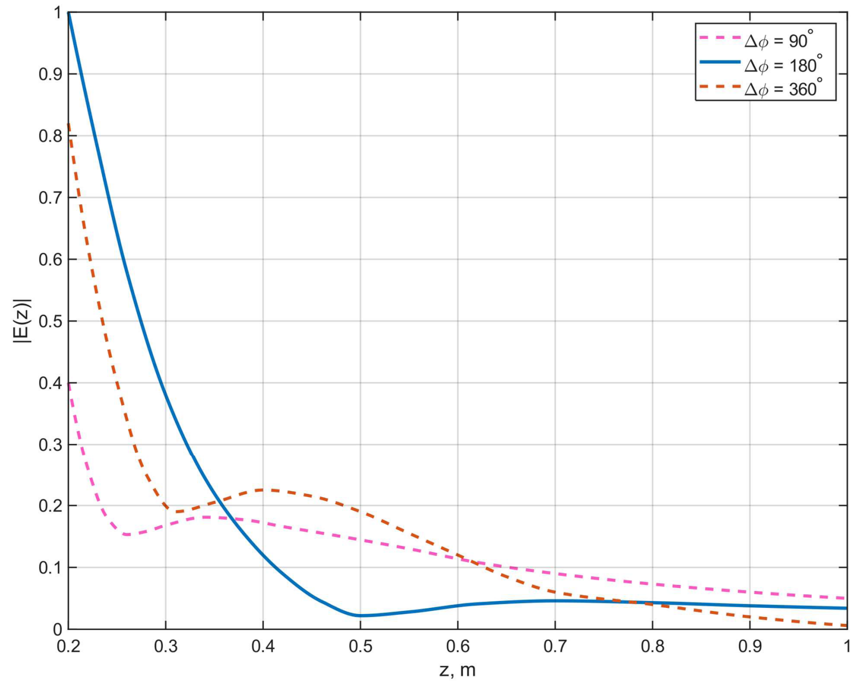

FIGURE 7. Dependencies of the electric-field strength amplitude taking into account the reflected wave from the scattering point.

Therefore, the resulting field at the k-th point is a superposition of complex amplitudes formed along the direct propagation path and as a result of reflection from the scattering point:

$$E_k^{(\Sigma)} = E_k^{(DP)} + E_k^{(BP)}. \tag{7}$$

We tested theoretical assumptions made using mathematical modeling. To do this, we constructed a model of the system shown in Figure 1. The antenna's operating frequency was 2.5 GHz; the transmitting antenna coordinates are ($x = 0; y = 0; z = 0$); and the receiving point coordinates were ($x = 0.5; y = 0; z = 0$). We will vary the scattering point coordinates so that as a result of re-reflection from it, the phase difference at the receiving point between $E_k^{(\mathrm{DP})}$ and $E_k^{(\mathrm{BP})}$ will be $\Delta\varphi = 90°$; $\Delta\varphi = 180°$; $\Delta\varphi = 360°$. For phase difference $\Delta\varphi = 90°$ the coordinates of the scattering point should be ($x = 0.25; y = -0.09; z = 0$); for $\Delta\varphi = 180°$, the coordinates of the scattering point should be ($x = 0.25; y = -0.125; z = 0$); for $\Delta\varphi = 360°$, the coordinates of the scattering point should be ($x = 0.25; y = -0.185; z = 0$). The reflection coefficient is taken to be equal to that of an ideal reflector, that is, $\Gamma = 1$.

Figure 7 shows results of the mathematical modeling for the three phase differences under consideration.

By analyzing the dependence of the electric-field strength amplitude on the distance obtained for the three phase differences, it can be observed that the simulation results coincide with the expected results:

- With a phase difference $\Delta\varphi = 180°$, destructive interference occurs. This means that the waves arriving at the receiving point are combined in an antiphase, resulting in a decrease in the electric-field strength amplitude at the receiving point.
- With a phase difference $\Delta\varphi = 360°$, constructive interference occurs. The waves at the receiving point add up in phase, leading to an increase in the amplitude of the electric-field strength near the receiving point.
- With a phase difference $\Delta\varphi = 90°$, interference addition of waves occurs. This is known as partial interference.

In addition, from the dependencies shown in Figure 7, it can be noted that with constructive and partial interference, the maximum amplitude of the electric-field strength is shifted towards the antenna relative to the reception point, which is because two phenomena are in conflict here: the in-phase addition of waves and the decrease in the intensity of the electric field with increasing distance r^{-q}. These phenomena balance each other before the reception point, and this effect is identical to the focusing of a multi-element linear antenna array due to the in-phase addition of waves at the required point in space [10]. In destructive interference, there are no opposing phenomena because the waves are added in antiphase (cancel each other), as well as a decrease in the intensity of the electric field with increasing distance r^{-q}; thus, the minimum electric-field strength is ensured exactly at the receiving point. **The results of mathematical modeling qualitatively coincided with those of the electrodynamic modeling.**

Because we represent the system of radiating antennas and receiving points as a microwave multiport, we recall that the S-parameters describe the relationship between the incident and reflected waves at ports of the multiport [11–13]. For an N-port multiport network, the amplitudes of the incident waves a_i and reflected waves b_i at each port i are introduced, which are connected by linear relations [9]:

$$b_i = \sum_{k=1}^{N} S_{i,k} \cdot a_k, \quad i = 1, 2, \dots, N, \tag{8}$$

where $S_{i,k}$ is the complex transfer coefficient between the k-th and i-th ports, when $k \neq i$.

In the presence of reflectors in the form of scattering points, elements $S_{i,k}$ must be supplemented. For example, if a scattering point b lies on the path from port k to port i, then it creates an addition to the transmission coefficient $S_{i,k}$. Considering all reflecting points B, the effective transmission coefficient can be expressed as follows:

$$S_{i,k}^{\mathit{eff}} = S_{i,k}^{(0)} + \sum_{b=1}^{B} S_{i,k}^{(b)}, \tag{9}$$

where $S_{i,k}^{(0)}$ is the original complex transmission coefficient, excluding scattering points, and $S_{i,k}^{(b)}$ is the contribution to the transmission coefficient from the b-th scattering point.

The addition in expression represents the coherent superposition of complex transmission contributions associated with different propagation paths. It should not be interpreted as an arbitrary addition of the scattering matrices of separate interconnected networks. Instead, each term $S_{i,k}^{(b)}$ is defined as the contribution of the b-th reflected path to the total transmission coefficient between ports k and i. Let only port k be excited by an incident wave with complex amplitude a_k. Owing to the linearity of Maxwell's equations, the outgoing wave at port i is the sum of the direct and reflected contributions: $b_i = b_i^{(0)} + \sum_{b=1}^{B} b_i^{(b)}$. The individual components can be written as $b_i^{(0)} = S_{i,k}^{(0)} \cdot a_k$, $b_i^{(b)} = S_{i,k}^{(b)} \cdot a_k$. Therefore, $b_i = (S_{i,k}^{(0)} + \sum_{b=1}^{B} S_{i,k}^{(B)}) a_k$. Dividing this relation by a_k gives effective transmission coefficient. This expression corresponds to the single-scattering approximation, in which the direct path and paths containing one reflection are retained, whereas multiple successive reflections and interactions between scattering objects are neglected.

Expression (9) is explained in terms of summing the original complex transmission coefficient and the contribution from the scattering point.

By adding scattering points to the system, additional signal pathways are created:

- The signal from port k reaches the scattering point b.
- The scattering point b reflects and re-radiates the signal towards port i.

Thus, for the wave traveling along the direct path, already taken into account, a new component is added, which considers the new path created by the scattering point. Because the system of S-parameters of a multipole is a linear system, the final amplitude is the sum of the contributions of the main path $S_{i,k}^{(0)}$ and all additional paths $S_{i,k}^{(b)}$.

Consider a wave incident from port k to port i and scattered by scattering point b. Within the generalized power-law attenuation model adopted in this work, the contribution of the b-th reflected path to the transmission coefficient is approximated as follows [14–16]:

$$S_{i,k}^{(b)} = F_{i,b} \cdot \Gamma_{b,k} \cdot (r_{i,b} + r_{b,k})^{-q} \cdot \exp\left(-j \cdot \beta \cdot (r_{b,i} + r_{k,b})\right), \tag{10}$$

where $\Gamma_{b,k}$ is the complex reflectivity between the b-th scattering point and the k-th port; r_{ib} is the distance between the i-th port and the b-th scattering point; and $r_{i,b}$ is the distance between the b-th scattering point and the k-th port.

The attenuation factor in Expression (10) is introduced within the generalized power-law model adopted in Expression (4). The reflected trajectory is represented as an equivalent propagation path with the total length. Accordingly, the amplitude attenuation along this path is approximated by (10). The exponent q is an effective field-amplitude decay exponent and should not be interpreted as a received-power path-loss exponent. This distinction is important when comparing Expression (10) with the Friis transmission formula. The Friis formula describes the ratio of received and transmitted powers between antennas under far-field free-space conditions, and Expression (10) describes a complex field-amplitude contribution to the transmission coefficient. For the near-field calculations considered in this work, $q = 2$ is used as an effective engineering approximation that represents a faster spatial variation of the field amplitude. It is not assumed to be a universal analytical law for all near-field configurations. The same approximation is used for both direct and reflected paths to maintain consistency in the adopted transmission-coefficient model. The use of this reduced power-law representation is justified by the objective of the present study, which is to analyze the relative changes in the field distribution and the phase compensation of the reflected component rather than to calculate an absolute link budget. The applicability of the underlying power-law field model to focused antenna arrays was experimentally examined in [17], where the calculated field distributions showed good agreement with measurements obtained using an antenna-array prototype. In the present work, the qualitative agreement between the mathematical and full-wave electrodynamic modelings additionally supports the use of this approximation for the considered single-reflection scenario.

In an idealized case, we consider scattering points as ideal mirror reflectors, that is, reflection occurs according to the mirror law, in which the angle of incidence is equal to the angle of reflection $\theta_{\text{inc}} = \theta_{\mathit{refl}}$.

Let us write down the condition for the modulus of the reflection coefficient for an ideal specular reflection:

$$|\Gamma(\theta)| = \begin{cases} 1, & \theta_{\text{inc}} = \theta_{\mathit{refl}} \\ 0, & \theta_{\text{inc}} \neq \theta_{\mathit{refl}} \end{cases}, \tag{11}$$

It should also be noted that the scattering-point model corresponds to the reflection's specular nature, in which the main energy of the reflected wave propagates along the direction determined by the law of equality of angles of incidence and reflection. Under real conditions, part of the energy may be scattered in other directions owing to the finite size of the object, surface roughness, material inhomogeneity, and complex geometry of the reflector. In this case, the contribution of the reflecting object can be described not by a single specular ray but by a set of elementary scattered components.

4. COMPENSATION FOR THE INFLUENCE OF A SCATTERING POINT

Mathematical modeling is necessary to verify the theoretical results presented in this study. Let us consider an antenna array consisting of $N = 3$ radiators, operating frequency $f = 2.5\,\text{GHz}$, the radiation pattern of a single emitter is assumed to be isotropic, the reception point is located at a distance of $0.5\,\text{m}$ from the antenna array, and the focal axis is located orthogonally to the geometric center of the antenna array. The step between the antenna array radiators was half the wavelength at the operating frequency $\lambda/2$. We will vary the coordinates of the scattering point so that as a result of re-reflection from it, the phase difference at the receiving point between the direct path from the central emitter $E^{(\text{DP})}$ and the reflected path from the central emitter $E^{(\text{BP})}$ through the scattering point is $\Delta\varphi = 180°$. For phase difference $\Delta\varphi = 180°$, coordinates of the scattering point should be $(x = 0.25; y = -0.125; z = 0)$. The reflection coefficient is taken to be equal to $\Gamma = 1$. Figure 8 shows a visual representation of this model.

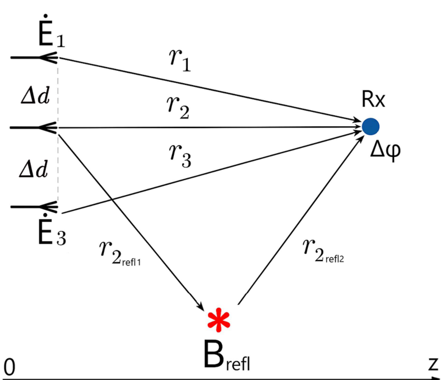

FIGURE 8. Model of a system consisting of an antenna array, a receiving point and a scattering point.

Let us calculate the distribution of the electric field in space for three cases:

1. The antenna array generated the maximum electric-field strength at the receiving point. There are no scattering points in the system.
2. A scattering point was introduced into the system, and a simulation was performed for the phase difference relative to the central emitter $\Delta\varphi = 180°$. The amplitudes and initial phases of the signals were calculated without considering the effective transmission coefficients (transmission coefficients that consider the influence of scattering points).
3. A simulation similar to that in point 2 was performed, but the amplitudes and initial phases of the signals were calculated considering the influence of effective transmission coefficients, which consider the influence of scattering points.

Using Expression (3), we calculated amplitudes and initial phases of the signals for the antenna array emitters for operation at a given receiving point, using direct transmission coefficients without considering multiple reflections (4) and using full transmission coefficients considering multiple reflections (9). The resulting amplitudes and initial phases of the signals are presented in Table 3.

Figure 9 shows the dependencies of the electric-field strength amplitude.

By analyzing the dependencies shown in Figure 9, it can be observed that introducing a reflecting object into the system that produces a phase difference of $\Delta\varphi = 180°$ between the signal from the central radiator and the reflected signal leads to a decrease in the electric-field strength amplitude in the vicinity of the receiving point. Considering this reflection in the S-parameter matrix (9) yields, as a solution of the system of equations (3), signal amplitudes and initial phases that make it possible to compensate for the influence of the scattering point on the resulting electric field strength in the vicinity of the receiving point. The absence of an increase in the amplitude of the electric-field strength at the receiving point is associated with a small size of the antenna array [10].

Table 4 presents the electric-field strength amplitude at receiving points.

The values in Table 4 show that after the compensation for the influence of scattering point, the electric-field strength amplitude at the receiving point increased by 49% and differed from the case without a scattering point by only 3%. This indicates the effectiveness of the proposed compensation method.

The increase in the electric-field strength after compensation is caused by recalculating amplitudes and initial phases of the signals supplied to the antenna-array radiators with an additional reflected propagation path taken into account. As a result, the direct and reflected field components are combined more favorably at the receiving point, reducing destructive interference and increasing the resulting field amplitude.

Let us consider the compensation for the same example but at an operating frequency of $5\,\text{GHz}$. Figure 10 shows the dependence of the electric field strength amplitude.

Analysis of the modeling results at a frequency of $5\,\text{GHz}$ shows that considering a reflected path in the transmission coefficient matrix also makes it possible to partially compensate for the influence of the scattering point; however, the restoration of the field amplitude at the receiving point is less accurate than at a frequency of $2.5\,\text{GHz}$. At shorter wavelengths, the same change in the propagation path length leads to a larger phase change. Consequently, the system becomes more sensitive to the position of the reflecting object and differences in the lengths of direct and reflected paths for individual radiators of the antenna array. In addition, the condition of a specified phase difference between the direct and reflected signals is satisfied for the selected radiator, for example the central one, whereas the phase relationships differ for the side radiators.

TABLE 3. Amplitudes and initial phases.

Radiator	a_n, V. Direct path matrix	φ_n, deg. Direct path matrix	a_n, V. Effective matrix	φ_n, deg. Effective matrix
1	0.575	72.3	0.748	116.4
2	0.583	61.5	0.122	62.1
3	0.575	72.3	0.653	32.0

TABLE 4. Electric-field strength amplitudes at the receiving point.

Configuration	Normalized field magnitude	Change relative to the uncompensated case
Without a reflector	0.3664	–
With a reflector, without compensation	0.2373	–
With a reflector, after compensation	0.3554	+49.8%

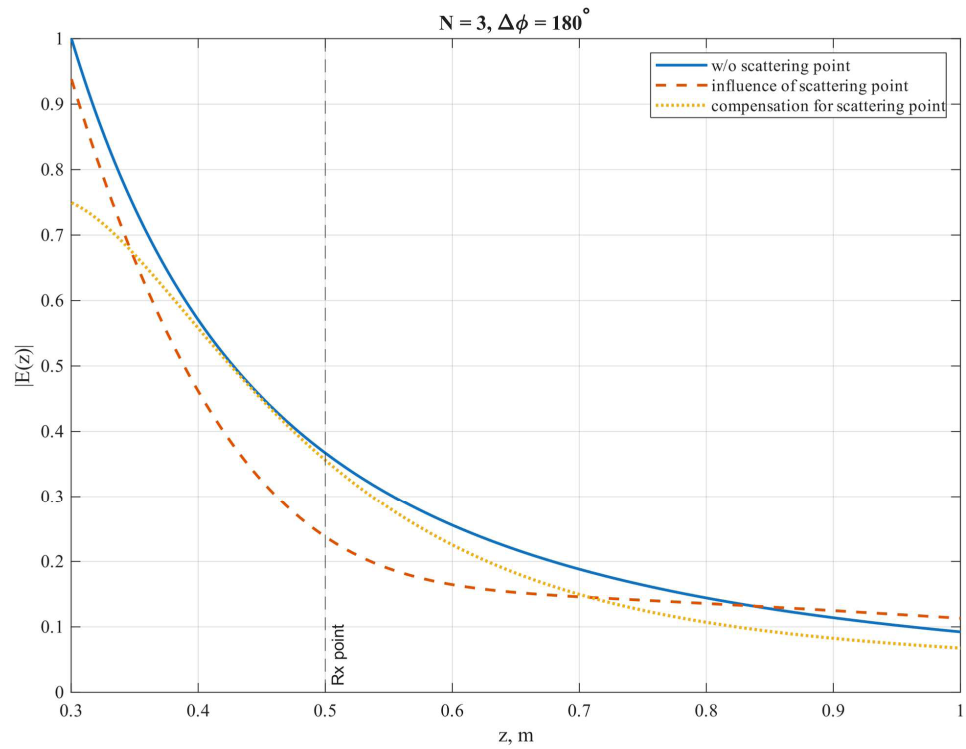

FIGURE 9. Electric-field strength amplitudes at a frequency of 2.5 GHz.

In this study, an idealized case of a single specular reflector represented as a scattering point was considered. This approximation makes it possible to explicitly trace the influence of the reflected path on the resulting field and verify the possibility of compensating for distortions by including the reflected path in the transmission coefficient matrix. However, this model has several limitations.

First, ideal reflection was assumed, in which the magnitude of the reflection coefficient was equal to unity. Under real conditions, the reflection coefficient is a complex quantity that depends on the object's material, frequency, angle of incidence, and wave polarization. Therefore, in the model's practical applications, it is necessary to use a reflection coefficient value determined analytically by electrodynamic modeling or experimentally.

Second, the study considers only a single reflection from a single object. In real rooms and confined spaces, several reflecting objects may be present, as well as multiple reflections between them. In this case, the effective transmission coefficient matrix should include the sum of the contributions from the direct path, single reflections, and, if necessary, higher-order paths.

Third, the reflecting object is represented as a scattering point; that is, its finite dimensions, shape, and possible diffuse scattering are not effectively considered. To accurately describe real objects, the reflector can be represented as a set of elementary scattering regions, each of which forms its own contribution to the resulting field.

Fourth, a three-element linear antenna array is considered as an example in this study. Increasing the number of radiators and moving to two-dimensional or three-dimensional antenna

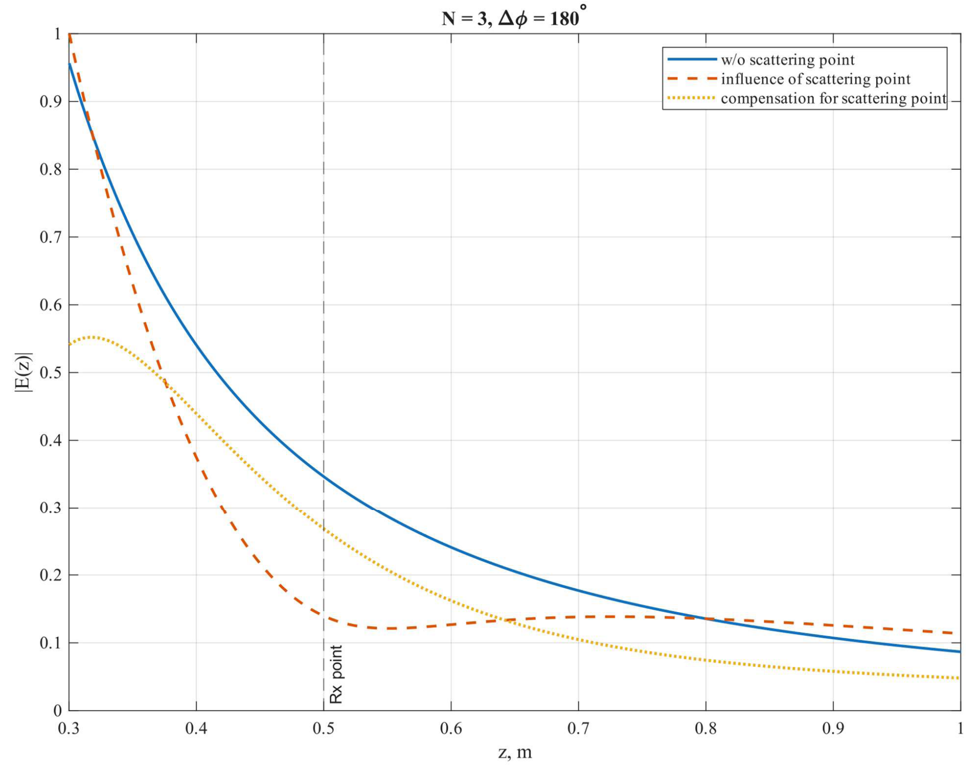

FIGURE 10. Electric-field strength amplitudes at a frequency of 5 GHz.

arrays can increase the system's degrees of freedom and consequently improve the possibility of compensating for field distortions in a specified region of space.

Thus, the proposed model is a basic first-order model. This demonstrates the fundamental possibility of accounting for the reflected path in the transmission coefficient matrix and can be used as a basis for further extension to more complex multipath scenarios.

5. CONCLUSION

This study considers the problem of accounting for a reflected propagation path when forming the required electromagnetic field distribution in space. A mathematical model is proposed, and contribution of the reflected path is included in the effective matrix of the complex transmission coefficients between the radiators of the antenna array and the receiving point. This approach makes it possible to account for the influence of the reflecting object at the stage of calculating the amplitudes and initial phases of the signals supplied to the radiators.

In the first stage, the cases of one radiator, one receiving point, and one scattering point were considered. It was shown that, under ideal specular reflection, changing the position of the reflector leads to a change in the phase difference between the direct and reflected waves, which in turn causes constructive or destructive interference at the receiving point. The results of the mathematical modeling are in agreement with those of the electrodynamic modeling.

In the second stage, a three-element antenna array was considered. It was shown that in the presence of a reflecting object, calculating the radiator excitations without considering the reflected path leads to a decrease in the field amplitude at the target point. Including the reflected path in the transmission coefficient matrix makes it possible to change amplitudes and initial phases of the signals such that the field amplitude at the receiving point becomes close to the initial case without a reflector.

It should be noted that the present study considers a basic idealized model of a single specular reflector. Further development of the approach is associated with considering the complex reflection coefficient, material losses, several reflecting objects, multiple reflections, diffuse scattering, and the analysis of the field distribution not only at a single point but also in a specified region of space. In addition, a promising direction is verification of the proposed model for antenna arrays with a larger number of radiators and more complex geometries that are close to real conditions of electromagnetic-wave propagation in indoor environments.

REFERENCES

[1] Natkaniec, M. and N. Bieryt, "An analysis of the mixed IEEE 802.11 ax wireless networks in the 5 GHz band," *Sensors*, Vol. 23, No. 10, 4964, 2023.

[2] Saha, R. K., "Coexistence of cellular and IEEE 802.11 technologies in unlicensed spectrum bands — A survey," *IEEE Open Journal of the Communications Society*, Vol. 2, 1996–2028, 2021.

[3] Cui, M., Z. Wu, Y. Lu, X. Wei, and L. Dai, "Near-field MIMO communications for 6G: Fundamentals, challenges, potentials, and future directions," *IEEE Communications Magazine*, Vol. 61, No. 1, 40–46, 2023.

[4] Zhang, H., N. Shlezinger, F. Guidi, D. Dardari, M. F. Imani, and Y. C. Eldar, "Beam focusing for near-field multiuser MIMO communications," *IEEE Transactions on Wireless Communications*, Vol. 21, No. 9, 7476–7490, 2022.

[5] Choi, H., J. Oh, J. Chung, G. C. Alexandropoulos, and J. Choi, "WiThRay: A versatile ray-tracing simulator for smart wireless environments," *IEEE Access*, Vol. 11, 56 822–56 845, 2023.

[6] Lerosey, G., J. d. Rosny, A. Tourin, A. Derode, G. Montaldo, and M. Fink, "Time reversal of electromagnetic waves," *Physical Review Letters*, Vol. 92, No. 19, 193904, 2004.

[7] Nguyen, H. T., J. B. Andersen, G. F. Pedersen, P. Kyritsi, and P. C. F. Eggers, "Time reversal in wireless communications: A measurement-based investigation," *IEEE Transactions on Wireless Communications*, Vol. 5, No. 8, 2242–2252, 2006.

[8] Basar, E., "Reconfigurable intelligent surfaces for doppler effect and multipath fading mitigation," *Frontiers in Communications and Networks*, Vol. 2, 672857, 2021.

[9] Iuzvik, D. and M. Stepanov, "Focusing of the electromagnetic field in several given areas of space," *Progress In Electromagnetics Research M*, Vol. 113, 11–22, 2022.

[10] Iuzvik, D. and M. Stepanov, "Ensuring the maximum amplitude of the electric field strength in given coordinates using a linear antenna array focused on a finite distance," *Journal of Electromagnetic Waves and Applications*, Vol. 38, No. 4, 411–427, 2024.

[11] Stimson, G. W., *Introduction to Airborne Radar*, SciTech Publishing, 1998.

[12] Säily, J. and A. V. Räisänen, *Studies on Specular and Non-Specular Reflectivities of Radar Absorbing Materials (RAM) at Submillimetre Wavelengths*, Helsinki University of Technology, Helsinki, Finland, 2003.

[13] Chau, J. L., J. M. Urco, J. P. Vierinen, R. A. Volz, M. Clahsen, N. Pfeffer, and J. Trautner, "Novel specular meteor radar systems using coherent MIMO techniques to study the mesosphere and lower thermosphere," *Atmospheric Measurement Techniques*, Vol. 12, No. 4, 2113–2127, 2019.

[14] Barrick, D. E., W. D. Stuart, and C. K. Krichbaum, *Radar Cross Section Handbook*, Plenum Press, 1970.

[15] Skolnik, M. I., *Introduction to Radar Systems*, McGraw-Hill, 1980.

[16] Pozar, D. M., *Microwave Engineering*, 4th ed., John Wiley & Sons, 2012.

[17] Sokolov, V., D. Iuzvik, and M. Stepanov, "Experimental evaluation of the possibility of positioning the maximum amplitude of the electric field strength at the required point in space," *International Journal of Sensors, Wireless Communications and Control*, Vol. 16, No. 2, 83–93, 2026.